Deductive geoacoustic inversion: Application to measurements in the Strait of Sicily

M. A. Ainslie, R. A. Laker, R. M. Hamson

CORDA Ltd, Apex Tower, 7 High Street, New Malden, Surrey, KT3 4LH, UK.
michael.ainslie@corda.co.uk, robert.laker@corda.co.uk, rachel.hamson@corda.co.uk

Abstract

A geoacoustic inversion model is applied to multitone transmissions from a towed source at Adventure Bank (Strait of Sicily) from the EnVerse 97 trial. The measured data, recorded on a vertical line array, are analysed using frequencies between 90 and 300 Hz and the results compared with inversions from other sources on the same data.

1. Introduction

The properties of the sea bed can have a dramatic effect on underwater acoustic propagation, especially in shallow water [1-4]. Direct measurement of sea bed properties over long distances is inevitably compromised by sparse sampling. Much attention has therefore been given in recent years to devising efficient inverse methods to obtain geoacoustic parameters from acoustic propagation measurements [5-7], hence providing average properties over longer ranges.

This paper describes some inversions carried out using DREAM [8, 9] on data from the EnVerse 97 trial in the Strait of Sicily [10]. The DREAM results are compared with inversions supplied by DERA using an evolutionary search algorithm (ESA) [11] and with results by TNO-FEL from Siderius *et al.* [10], using a genetic algorithm (GA). All three methods use a Bartlett processor, with either a parabolic equation forward model (ESA) or normal modes (DREAM and GA).

2. The EnVerse 97 Experiment

2.1 Trial Overview

An acoustic trial ('EnVerse 97' [10,12]) was carried out in October 1997 jointly by SACLANTCEN, TNO-FEL and DERA in Adventure Bank (Strait of Sicily). The objective of the trial was to assess the feasibility of measuring sea bed parameters acoustically using a towed source and fixed vertical line array (VLA) receiver. The array consisted of 64 hydrophones spaced at between 0.5 and 2.0 m and spanning 62 m in total. A sequence of tones, multitones and FM sweeps were recorded on the VLA at a distance of a few km from the towed source [10,12]. The inversions presented here are from a one minute multitone transmission, including the four frequencies 90, 130, 200 and 300 Hz. The distance between the array and towship at the start of transmission was approximately 1.7 km, increasing with time at a rate of about 1.6 m/s.

2.2 Environmental Conditions

The sound speed profile was measured using an expendable velocimeter probe two minutes after the multitone transmission [12] and decreases monotonically with depth from 1528 m/s at the sea surface to 1512 m/s at the sea bed. The water depth increases from about 98 m at the source to 102 m at the array. The measured wind speed was 5 m/s. The sea bed is described by Colantoni *et al.* [13] as "smooth sea-floor scarcely penetrated by acoustic energy (biogenic sands)" to the north of the array and "rough sea-floor not penetrated by acoustic energy (calcarenites with sandy spots and morphological highs, mostly rocky)" to the south. The current direction was towards the south east [12], causing the top of the array to tilt away from the source.

TG Leighton, GJ Heald, HD Griffiths, G Griffiths, (eds.), 'Acoustical Oceanography', Proc. Institute of Acoustics Vol. 23 Part 2, 2001.

3. Inversion Method and Sea Bed Parametrisation

Inversions are carried out using the DREAM (v3.3) program [9], using data recorded between 15:26:05 and 15:27:05 on 23 October 1997. The recording was divided into 20 successive 3 s snapshots and each snapshot was filtered to obtain amplitude and phase at each hydrophone for the desired frequencies. Our results are for a sequence of 17 consecutive snapshots between 15:26:08 and 15:26:59. DREAM inverts for up to 14 unknown parameters, 9 of which categorise the sea bed. Here we choose to solve for 13 parameters, keeping the water depth fixed at its value measured at the receiving array. The sediment is described by 6 of the 13 parameters (sediment thickness, surface sound speed, sound speed gradient, sound speed curvature, density and attenuation – see reference [8] for a complete description of the sediment profile) and a further 3 describe a uniform substrate (sound speed, density and attenuation). The remaining 4 are associated with the geometry (range and depth of the source, array depth and array tilt angle).

Because the water depth at the receiver is greater than the average along the transmission path, this approach is expected to overestimate the source range as explained in the appendix. However the geoacoustic inversion is thought to be robust to such geometrical errors provided that the assumed water depth is close to the true water depth [9].

4. Results

A summary table of inversion results, averaged over the 17 snapshots, is provided in Table 1, including a comparison with similar averages from two other sources. The DREAM inversions use 3 of the 4 frequencies mentioned in section 2.1 (90, 200 and 300 Hz). ESA and GA inversions use all 4 frequencies. Before solving for sea bed parameters it is first necessary to invert for pertinent geometric parameters, and these are discussed first.

	DREAM	ESA [14]	GA [10]
r_s (m)	1629[8]±27	1613[8]±28	-[4]
z_s (m)	51.6[9]±1.5	51.4[9]±1.4	-[4]
h_a (m)[5]	12.2±0.2	12.3±0.2	11.5±0.8
ϕ_a (°)[6]	1.27±0.08	1.27±0.05	1.37±0.17 [15]
h_{sed} (m)	14.6±15.7	25.9±8.8	31±12
c_0 (m/s)	1585±35	1632±26	1641±16
c' (/s)	11±6	5±5	3.4[2]
χ	−2.2±1.3	0.0[1]	0.0[1]
ρ_{sed} (g/cm^3)	1.60±0.11	1.32±0.10	1.46±0.18
α_{sed} (dB/λ)	0.72±0.37	0.25±0.05	0.43±0.16
c_{hsp} (m/s)	1780±122	1702±89	1813±51
ρ_{hsp} (g/cm^3)	1.87±0.15	1.40±0.42	1.46[3]
α_{hsp} (dB/ λ)	0.12±0.07	0.25±0.13	0.43[3]
Fitness[7]	0.936±0.014	0.958±0.008	-[4]

Table 1. Average (all snapshots) ± standard deviation

(1) Fixed at zero
(2) Calculated from average of c_{sed} (0), $c_{sed}(h_{sed})$ and h_{sed}
(3) Fixed at value in sediment
(4) Not available from reference [10]
(5) Height of bottom hydrophone from sea bed
(6) In-plane tilt angle from vertical
(7) Bartlett processor power
(8) Image source range (r_s')
(9) Image source depth (z_s')

4.1 Geometric Parameters

In principle the geometric parameters can be measured directly but in practice it is more convenient to solve for them as part of the inversion process. The array geometry is found to be stable over the one minute transmission with standard deviations of just 0.2 m in depth and 0.1° in tilt angle from vertical (see Table 1). Much larger variations in the source position are found and these are to be expected because the source is moving. A comparison with the expected source trajectory is made in section 5.1.2.

4.2 Geoacoustic Parameters

Before examining the results for individual parameters it is useful to analyse the behaviour of the sea bed profile as a whole. The inverted profiles form three clusters with distinct properties and Figure 1 shows the three best (highest fitness) profiles from each cluster. The main group comprises 10 snapshots (cluster A, indicated by solid lines) and is characterised primarily by a thin sediment (h_{sed} < 10 m) and a low half-space speed (c_{hsp} < 1705 m/s). A second group of 4 snapshots (cluster B, dashed lines) all have thick sediments (h_{sed} > 25 m), low surface sound speeds (c_0 < 1585 m/s) and high gradients (c' > 10 /s). The third group of 3 (cluster C, dotted lines) have moderate to large sediment thickness (h_{sed} > 15 m), high surface sound speeds (c_0 > 1600 m/s) and relatively low gradients (c' < 10 /s). Although we have not calculated statistics for each cluster, it is clear from Figure 1 that for some parameters at least (e.g. h_{sed}, c_0, c' and c_{hsp}) the standard deviations are much smaller than those indicated by Table 1 for all snapshots together.

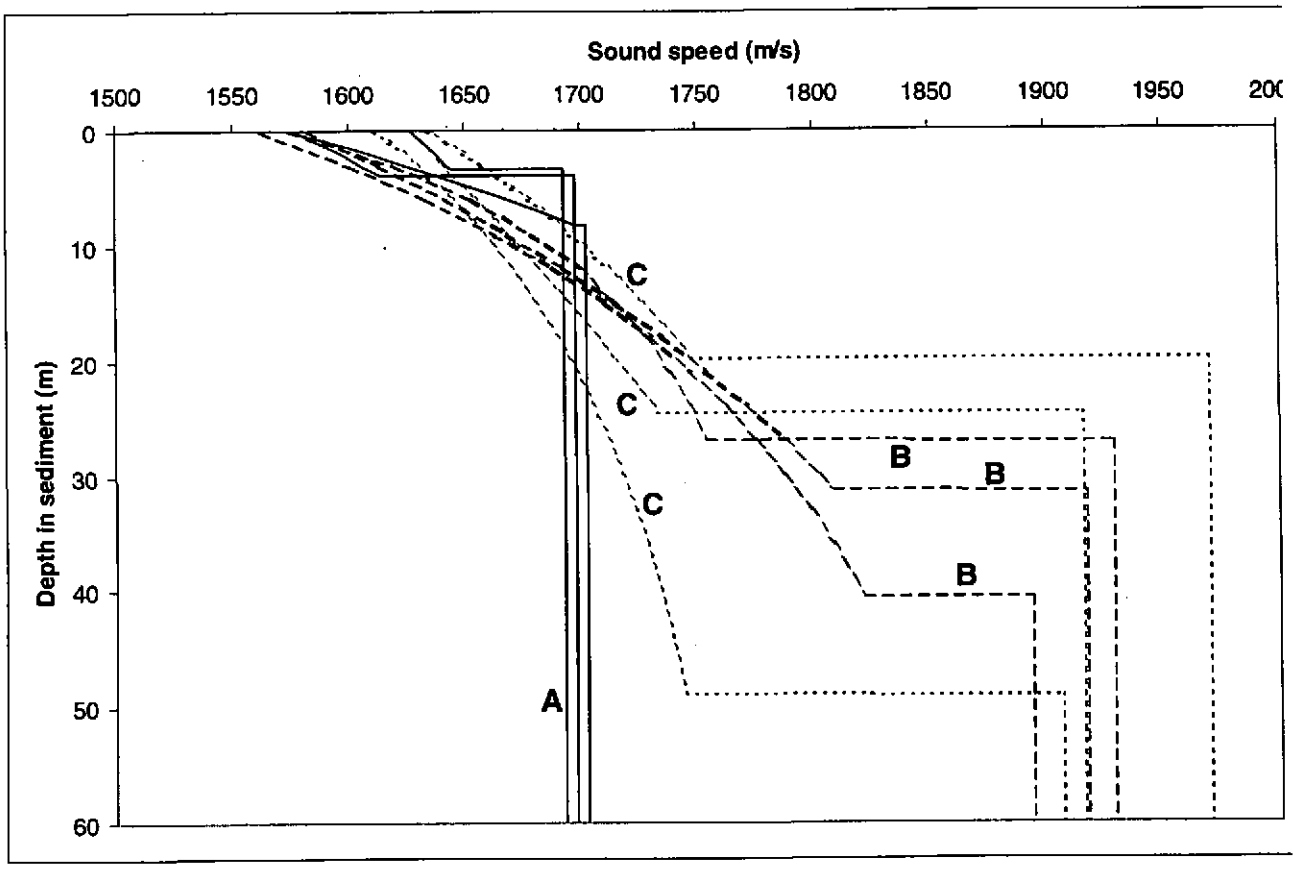

Figure 1. Best profiles from each cluster. Solid lines: cluster A; dashed lines: cluster B; dotted lines: cluster C.

5. Comparisons with Evolutionary Algorithms

Comparisons are made with inversions by two different evolutionary algorithm codes on the same one minute multitone recording. The first, and most direct, comparison is with ESA inversions using the same sequence of 3s snapshots [14]. The second is with GA results using a 1s snapshot time interval [10]. An important difference is that the DREAM inversions assume a fixed water depth, set at the value measured at the receiving array, whereas ESA and GA both search for the water depth. Because the inverted water depth and source range are highly correlated [16], the source range (and depth) found by the ESA and GA searches are not directly comparable with the DREAM values. To compensate for this a scaling factor can be applied to appropriate geometric parameters as specified in the appendix. All ESA values shown below, and in Table 1 above, include this scaling factor. As a result we expect to overestimate the true range by up to 60 m (see appendix). Unlike DREAM, both ESA and GA inversions use all four frequencies mentioned in section 2.1. Another difference is that DREAM uses data from 28 equally spaced hydrophones spanning 54 m, whereas the ESA and GA inversions use all 64 hydrophones (spanning 62 m).

5.1 ESA Comparisons (all snapshots)

5.1.2 Geometric data

Figure 2 compares DREAM and ESA inverted geometric parameters for all 17 snapshots (numbered 2 to 18). For the array parameters there is near perfect agreement: tilt angle of 1.3° and array height (from the sea bed) of 12 m. There is excellent agreement also for the source depth (average 51.5 m, decreasing at a rate of 6 m/minute). An independent (pressure sensor) measurement of the source depth gave a value of approximately 49 m, decreasing at 5 m/minute [14]. The accuracy of the pressure sensor is not known. Finally the inverted source ranges are in agreement to within 20 m, with both DREAM and ESA inversions indicating an average (horizontal) source speed of about 1.8 m/s, decelerating slightly during the 1 minute sequence.

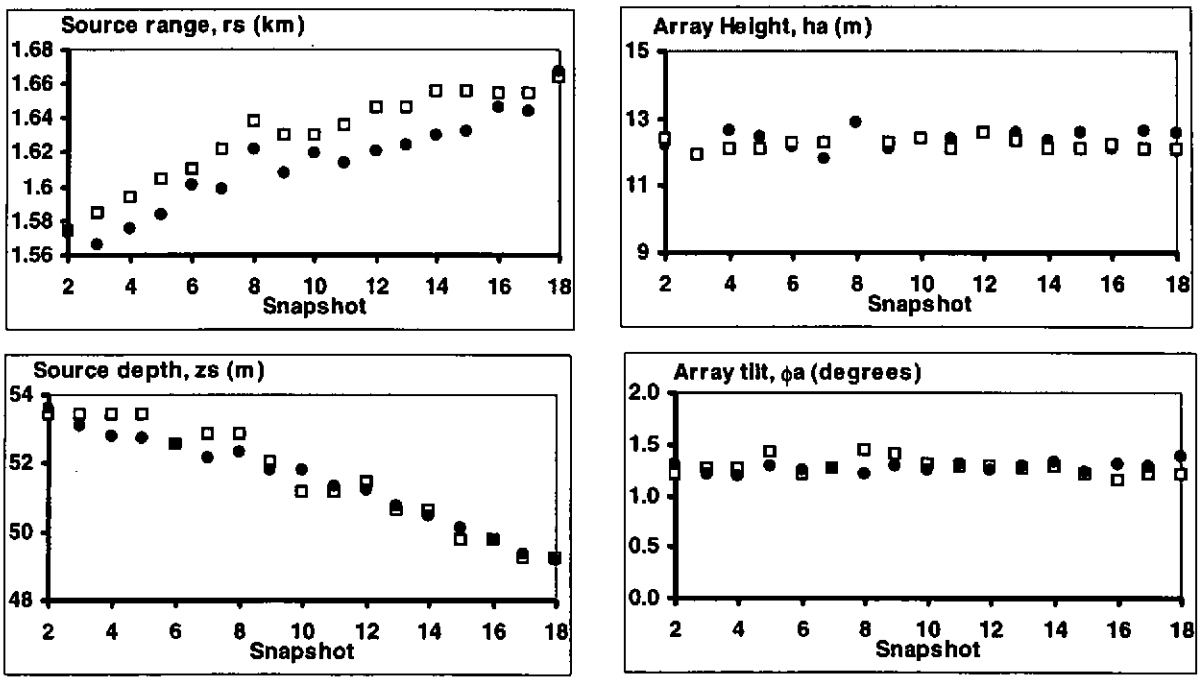

Figure 2. Geometric data: comparison between DREAM (squares) and ESA (circles).

	DREAM	ESA [14]	GA [10]
Δr_s (m)	$40^{(1)}\pm8$	$23^{(1)}\pm8$	$33^{(3)}\pm72$
Δz_s (m)	$0.6^{(1)}\pm0.4$	$0.5^{(1)}\pm0.2$	$1.8^{(2)}\pm1.9$
Δh_a (m)	3.7±0.2	3.8±0.2	$3.0^{(2)}\pm0.8$
$\Delta\phi_a$ (°)	−1.7±0.1	−1.7±0.1	−1.6 ±0.2 [15]

(1) Difference between inverted and expected image source position

$\Delta r_s = \langle (r_s')_{\text{inverted}} - (r_s')_{\text{expected}} \rangle$

$\Delta z_s = \langle (z_s')_{\text{inverted}} - (z_s')_{\text{expected}} \rangle$

(2) From Table 3 of reference [10]

(3) Value from Table 3 of reference [10] minus 25 m to enable a direct comparison with DREAM and ESA. This is to compensate for likely departures from a taut tow–cable [12].

Table 2. Comparison with expected geometry. In each case the tabulated value is the difference between the inverted value and the expected value (see Table 3), averaged over all snapshots.

A quantitative comparison between the expected and inverted source trajectory and array geometry is summarised in Table 2. Notice the small standard deviation in Δr_s and Δz_s (for DREAM and ESA) compared with Table 1. This is the residual standard deviation after allowing for the motion of the source. The values of Δr_s and Δz_s are smaller than the uncertainty in the measurements (Table 3). But there are significant unexplained discrepancies in both h_a and ϕ_a.

Time	r_s (m)	r_s' (m)	z_s (m)	z_s' (m)	h_a(m)	ϕ_a(°)
15:26:00	1513±25	1544±40	52.0	53.5±0.5	8.5±0.5	3±1
15:27:00	1610±25	1641±40	46.7	47.2±0.5	8.5±0.5	3±1

Table 3. Scaled and unscaled measurements (expected values of r_s, r_s' etc) used in the construction of Table 2. The time–varying parameters r_s and z_s are interpolated linearly between the times quoted for comparison with each snapshot.

5.1.3 Geoacoustic data

5.1.3.1 Sound speed profile

Comparison of geoacoustic parameters is complicated by the clustering behaviour observed in Section 4.2 above. With the exception of snapshot 8 (see Figure 3) the ESA sound speeds (c_0 values) are all higher than the median DREAM value, and this is compensated for by significantly lower sound speed gradients (c' values). Notice that 14 of the 17 ESA snapshots meet the criteria for cluster C (joined by dotted lines in Figure 3); notice in particular the consistency in c_0 and c' values for this cluster. Of the other three, snapshot 6 meets the criteria for cluster A, as would snapshot 2 if the sediment thickness criterion were relaxed to $h_{sed} < 15$ m. Similarly snapshot 8 meets the criteria for cluster B except for a relatively thin sediment. We hypothesise that the ESA might have found a thicker sediment for snapshot 8, and more solutions closer to cluster B generally, had departures been considered from zero curvature.

5.1.3.2 Attenuation and density

The sediment attenuation (α_{sed}) values found by DREAM are significantly higher than almost all of the ESA values for this parameter, and there appears to be a correlation with the gradient c'. It is possible that low values of c', which might otherwise result in an artificially high reflection loss, are being compensated for by low values of α_{sed}, and *vice–versa*. A more complete understanding of this behaviour may require variations of α_{sed} either in depth [17] or in frequency [18].

A high correlation is expected, and observed, between DREAM sediment density and sound speed values, due to the inversion method [9]. The ESA density values are consistently lower than those from DREAM.

5.2 GA Comparisons (averages)

A snapshot-by-snapshot comparison with the GA inversions is not possible because of the different time intervals used. We make the following observations concerning the average data from Tables 1 and 2:

5.2.1 Geometric data

The source position, array tilt and array height found by the GA are consistent with those from DREAM (and ESA) but with higher standard deviations although there is a significant and unresolved discrepancy with the expected array height (see Table 2). We believe the low standard deviations for DREAM are a consequence of having fixed the water depth. This lower standard deviation does not imply greater accuracy because of the uncertainty in the measured bathymetry (see appendix).

5.2.2 Geoacoustic data

The average geoacoustic data meet the criteria for cluster C (as do the ESA average data). The DREAM averages for cluster C only ($h_{sed} = 31 \pm 16$ m, $c_0 = 1624 \pm 12$ m/s, $c' = 6.3 \pm 1.5$ /s and $\alpha_{sed} = 0.55 \pm 0.28$ dB/λ) are similar to both GA and ESA results.

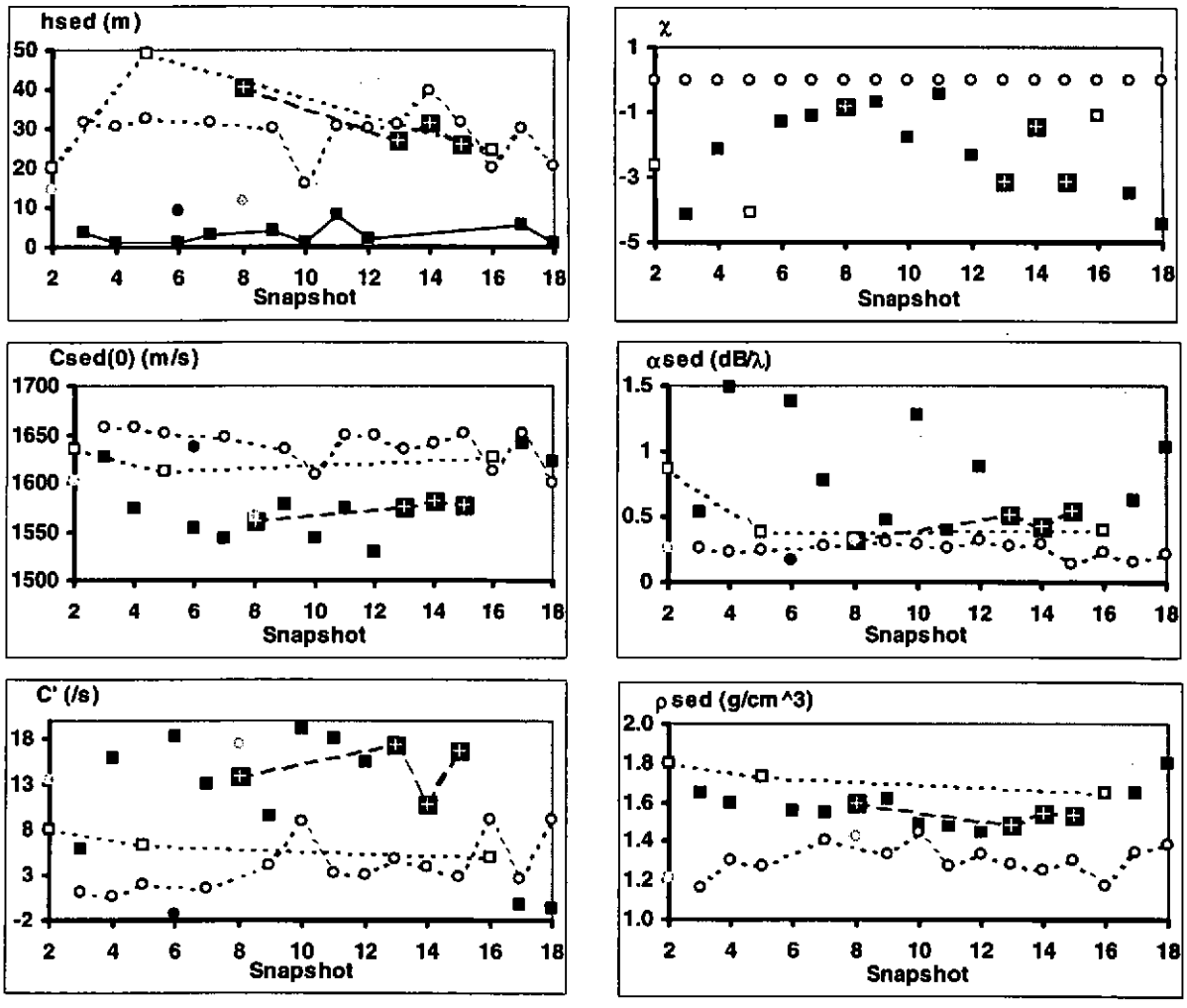

Figure 3. Geoacoustic data - comparison between DREAM (squares) and ESA (circles): sediment parameters. Clusters are indicated by the following symbols: Black square or black circle=cluster A; square with cross inside=cluster B; open square or open circle=cluster C; grey circle=outside cluster bounds. Where appropriate, correlations are emphasised by joining individual points from a cluster with the same line types as in Figure 1.

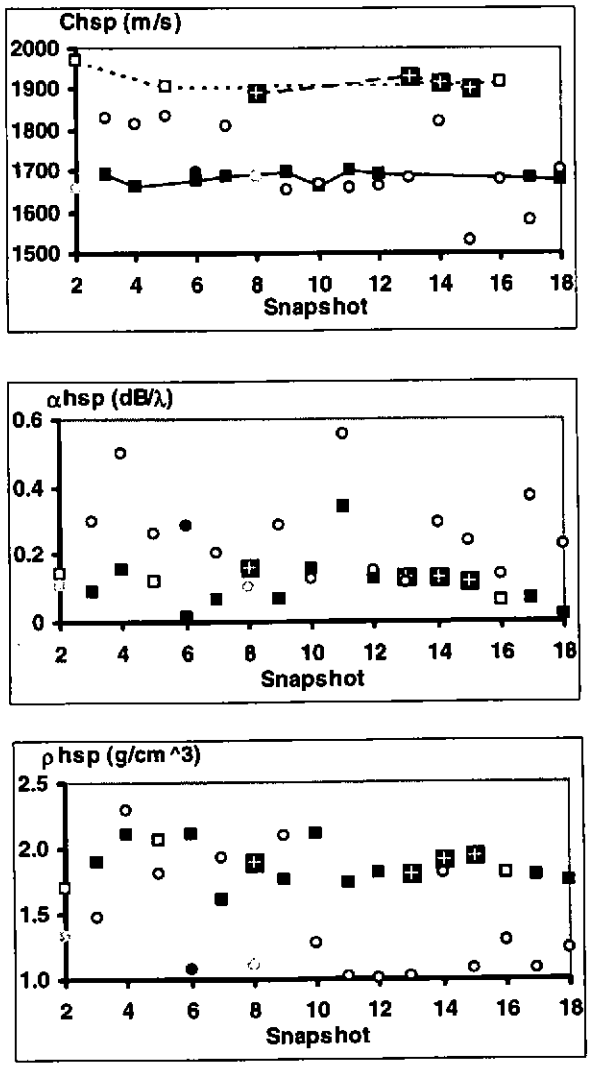

Figure 4. Geoacoustic data – comparison between DREAM (squares) and ESA (circles): half-space parameters. Clusters are indicated by the following symbols: black square or black circle=cluster A; square with cross inside=cluster B; open square or open circle=cluster C; grey circle=outside cluster bounds. Where appropriate, correlations are emphasised by joining individual points from a cluster with the same line types as in Figure 1.

6. Discussion and Conclusions

Inversion results for a moving source for the EnVerse 97 trial are presented. Stable geometric parameters are found for the source position and array geometry. The inverted source speed (1.8 m/s) is slightly higher than the tow speed (1.6 m/s) implying that the towed source may be catching up with the ship. If so, this would explain the apparent deceleration noted in section 5.1.2.

The geoacoustic data are much less clear cut and form three distinct clusters. One of these (cluster C) is very similar to GA inversions on the same data set. The other two clusters have either a much thinner sediment (cluster A) or a lower sound speed and higher gradient (cluster B). This clustering makes interpretation difficult but we believe that it points to a need for greater sophistication in the sediment model. Available seismic records [10] suggest significant variation with range along the track. Or perhaps there is actually a thin near-surface layer, overlying a deeper layer with a higher sound speed.

7. Acknowledgements

Thanks are due to M Lee and D Miles of DERA for making available copies of their filtered acoustic data and inversion results, and to S Smithers of CORDA for typing and formatting. Acoustic and environmental measurements were made by NRV Alliance (SACLANTCEN) and HNLMS Tydeman (RNN).

Appendix – Image Source Position

The purpose of this appendix is to explain the distinction between the source position (r_s, z_s) and the apparent (or image) source position (r_s', z_s'). We define the image source as that which, placed in a range-independent ocean of depth H', reproduces (approximately) the same acoustic field as the true source in the true (range-dependent) environment. The relationship between them is [16]:

$$r_s' = r_s H'^2 / H_e^2 \qquad \text{and} \qquad z_s' = z_s H' / H_s \tag{1}$$

where H_e is an effective water depth, approximately equal to the average water depth between source and receiver [9,16] and H_s is the actual water depth at the source.

For the case in hand we have H' =101.5 m (the water depth assumed for our inversions), H_s=98.5±1 m and H_e=100.5±1 m (estimated from the measured bathymetry), so that

$$r_s'/r_s = 1.02 \pm 0.02 \qquad \text{and} \qquad z_s'/z_s = 1.03 \pm 0.01$$

References

[1] Pace NG (ed). Acoustics and the Sea-Bed (Bath University Press, Bath, 1983).

[2] Lara Sáenz A, Ranz Guerra C and Carbó Fité C (eds). Acoustics and Ocean Bottom (Consejo Superior de Investigaciones Científicas, Madrid, 1987).

[3] Hovem JM, Richardson MD and Stoll RD (eds). Shear Waves in Marine Sediments (Kluwer, Dordrecht, 1991).

[4] Pace NG and Langhorne DN (eds). Acoustic Classification and Mapping of the Seabed (Institute of Acoustics, St Albans, 1993).

[5] Diachok O, Caiti A, Gerstoft P and Schmidt H (eds). Full Field Inversion Methods in Ocean Seismo-Acoustics (Kluwer, Dordrecht, 1995).

[6] Chapman NR and Tolstoy A (eds). Benchmarking Geoacoustic Inversion Methods, Special issue of J. Comp. Acoust. Vol 6, March and June 1998.

[7] Taroudakis M (ed). *Proc 1st Workshop on Inverse Problems in Underwater Acoustics*, Heraklion, Greece, May 1999.

[8] Ainslie MA, Hamson RM, Horsley GD, James AR, Laker RA, Lee MA, Miles DA and Richards SD. Deductive multi-tone inversion of seabed parameters. *J. Comp. Acoust.* 2000; **8**(2): 1-15.

[9] Ainslie MA and Laker RA. Deductive geoacoustic inversion: Robustness to water depth mismatch, in *'Acoustical Oceanography', Proceedings of the Institute of Acoustics Vol. 23 Part 2, 2001*, T G Leighton, G J Heald , H Griffiths and G Griffiths, (eds.), Institute of Acoustics, (this volume), pp. 60-65.

[10] Siderius M, Snellen M, Simons DG and Onken R. An environmental assessment in the Strait of Sicily: Measurement and analysis techniques for determining bottom and oceanographic properties. *J. Oceanic Eng.* 2000; **25** (3): 364-386.

[11] Lee MA and Miles DA. Unpublished DERA Report, 2000.

[12] Snellen M and Simons DG. The EnVerse 97 Matched Field Processing sea trial, TNO report FEL-99-A127, July 1999.

[13] Colantoni P, Ligi M, Morsiani MP and Penitenti D. Morphology and recent sedimentary evolution of the western Sicilian continental shelf, Ed Max MD and Colantoni P, UNESCO Reports in Marine Science **58**, 93-98 (1993).

[14] Lee MA. Personal communications, August and September 2000.

[15] Snellen M. Personal communication, January 2001.

[16] Harrison CH and Siderius M. Correlations between search parameters in geoacoustic inversion, in *Proceedings of the fifth European Conference on Underwater Acoustics*, P Chevret P and ME Zakharia (eds.) Lyon, France, 2000.

[17] Mitchell SK and Focke KC. The role of the seabottom attenuation profile in shallow water acoustic propagation, *J. Acoust. Soc. Am.* 1983; **73**: 465-473.

[18] Kibblewhite AC. Attenuation of sound in marine sediments: A review with emphasis on new low-frequency data, *J. Acoust. Soc. Am.* 1983; **86**: 716-738.

Deduction of seabed type using in-water acoustic measurements

M. K. Prior[1], S. G. Marks[2]

[1] DERA Winfrith, Dorchester Dorset, DT2 8XJ, UK. mkprior@dera.gov.uk
[2] DERA Unit, Southampton Oceanography Centre, Southampton, S014 3ZH, UK. s.marks@soc.soton.ac.uk

Abstract

Nine descriptions of the geoacoustic structure of the seabed are developed to provide a good, broad description of conditions that will be present in many ocean environments. A method is then developed that allows measurements of underwater acoustic propagation loss to be used to invert for the seabed type present in the region in which the measurements are made. The method is tested using measured propagation loss from the Northwest approaches to the UK. At frequencies of 150 Hz and 400 Hz, the results of the inversion method are shown to agree with geoacoustic data derived from seabed cores taken in the same area. Inversions at higher frequencies are shown to be less reliable than the lower frequency inversions, and possible reasons for this are discussed.

1. Introduction

Interaction between sound and the seabed can be strong, especially in shallow water regions. Any uncertainty in the description of the seabed's geological structure results in uncertain predictions of sonar performance. One way of filling this gap in knowledge is to use measured acoustic signals to determine the structure of the seabed. Methods have been developed to attempt this [1], but many of these techniques have been designed to use research sonars and could not be implemented with non-specialist equipment. There would be great benefit if a method could be developed that allowed the seabed to be determined from acoustic measurements made routinely by seagoing platforms with non-specialist sonars.

Although it is highly desirable to develop detailed models and databases of the seabed to support acoustic propagation modelling, it would take significant effort to do so globally, at resolutions suitable for routine propagation loss calculations. It is therefore more practical, for the purposes of inversion modelling, to use a pragmatic approach and to design robust seabed models, which represent key features of the seabed. These robust models can be used as the basis of a pragmatic acoustic inversion method that allows the seabed to be classified as being most similar to one of a limited number of seabed types.

This paper describes the production of robust seabed models that should cover the majority of seabed types found throughout the world's oceans. It then describes an acoustic inversion method suitable for determining which of the seabed models gives the best fit between measured and modelled acoustic propagation loss. The application of this method to an acoustic dataset, measured in the Northwest approaches to the UK, is then described, and the seabed type produced by the inverse method is compared with seabed data gathered from cores in the same area.

2. Seabed Models

The requirement for the development of seabed models is a set of parameter-depth curves which provide a regular incremental spacing in one parameter, i.e. curves representing seabeds with regularly changing values of parameter "x". It has been identified [2] that porosity strongly controls geoacoustic properties of sediments, particularly fine-grained sediments, and so the models are based on porosity. The fine grained sediment models are arguably the most important, as although about 71% of surficial sediments are sand, they are usually less than 1m thick and, where known, about two thirds of the underlying Quaternary sediment around the UK is predominantly fine-grained [3].

The approach adopted is therefore to produce a series of seabed models representing regular increases in porosity. These start from rock, move through coarse grained sediments, and end with very fine grained mud. It is found that in adopting this approach, the number of models required is nine. These are now described in order of increasing grain size.

TG Leighton, GJ Heald, HD Griffiths, G Griffiths, (eds.), 'Acoustical Oceanography', Proc. Institute of Acoustics Vol. 23 Part 2, 2001.

2.1 Fine-grained sediments (models 5 to 9)

The Baldwin and Butler [2] relationship between porosity and depth is used to model fine-grained sediments and is:

$$D = 6.02 * (1 - \phi)^{6.35} \quad (1)$$

where D is the depth below the seabed in km and ϕ is the fractional porosity. From the porosity, it is possible to calculate directly the density, using the following relationship:

$$\rho_{sediment} = \rho_{grain}(1-\phi) + \rho_{water}\phi \quad (2)$$

where $\rho_{sediment}$ is the density of the fluid saturated sediment (kgm^{-3}), ρ_{grain} is the density of the sediment grains (kgm^{-3}) and ρ_{water} is the density of the pore water (kgm^{-3}). For most terrigenous sediments, a grain density of 2650 kgm^{-3} can be used and the density of water can be approximated by 1000 kgm^{-3}. It has been shown [4] that the compressional wave versus depth relationship could most simply be represented by the relationship:

$$V_p(d) = [V_{p0}^{\ 2}(1+\beta)^2 + 2(1+\beta)g.V_{p0}.d]^{1/2} - \beta V_{p0} \quad (3)$$

where $V_p(d)$ is the velocity with depth d, below the seabed in metres, V_{p0} is the velocity of the sediment at the seabed, g is a gradient parameter (8.603 s^{-1}) and β is a dimensionless curvature parameter (-0.933).

The GEOSEIS algorithms [5, 6] provide values of attenuation for sediments and these have been used in this study. To create models to represent fine grained sediments of higher and lower porosity at the same depth, the porosity/depth relationship is given the same curvature, but shifted by a value of 10% porosity for each of the new models. To cover a wide porosity/depth field, four additional curves have been derived, one with higher porosity and three with lower porosities than the original [2] model. Figure 1 shows the model curves plotted with porosity measurements obtained from sediment cores. The data points show some scatter, but the decrease in porosity with depth seems to match the curvature of the models.

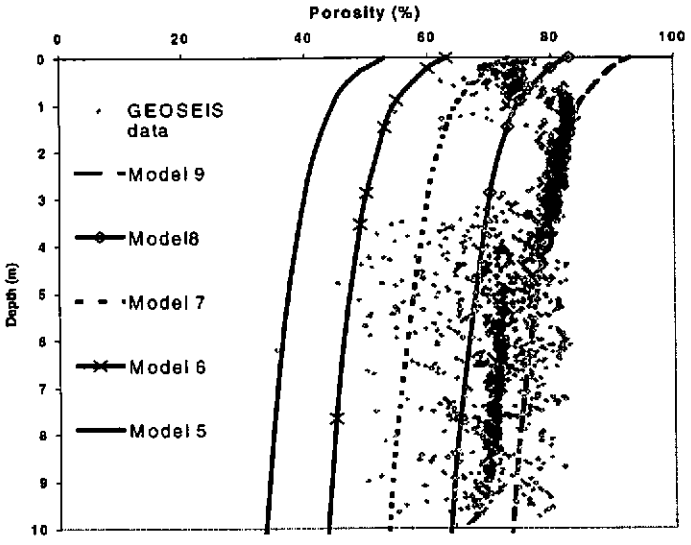

Figure 1. Porosity-depth relations for fine-grained sediment

2.2 Coarse-Grained Sediment Models (model numbers 2-4)

An alternative approach is taken for the coarse grained sediments, because they lithify differently from fine-grained muds and so have different depth dependencies. It has been shown [4] that the porosity/depth relationships in the literature [7] were less satisfactory for sands than the Baldwin and Butler [3] relationship for muds. For this study, the GEOSEIS velocity/depth and velocity/porosity relationships have been used to derive a porosity/depth relationship:

$$n = n_s + 0.158d \quad (4)$$

where d is depth below the seabed, measured in metres, n is the percentage porosity and n_s is the percentage porosity at the seabed. The histogram for sand (Figure 2) indicates that the most common porosities are concentrated between 35% and 55%. Using the above relationships, two sand models are created, with n_s of 49% (the maximum value recommended by [7]) and n_s of 40%. Density with depth was calculated from porosity using (2) and the velocity and attenuation profiles were derived from the GEOSEIS algorithms [6].

Gravel porosities are very similar to those of sands (see Figure 2). A gravel model was derived using the lower sand porosity/depth relationship and from that relationship, density was calculated. The GEOSEIS algorithms for gravels were used to calculate velocity and attenuation.

The porosity/depth curves for the sand and gravel models are plotted with sand and gravel sediment data from GEOSEIS (Figure 3). Most of the data are equivalent to values at the seabed but indicate the range of porosities for coarse-grained data. The dataset which shows the variation of porosity with depth [8] indicates a general trend of decreasing porosity with depth.

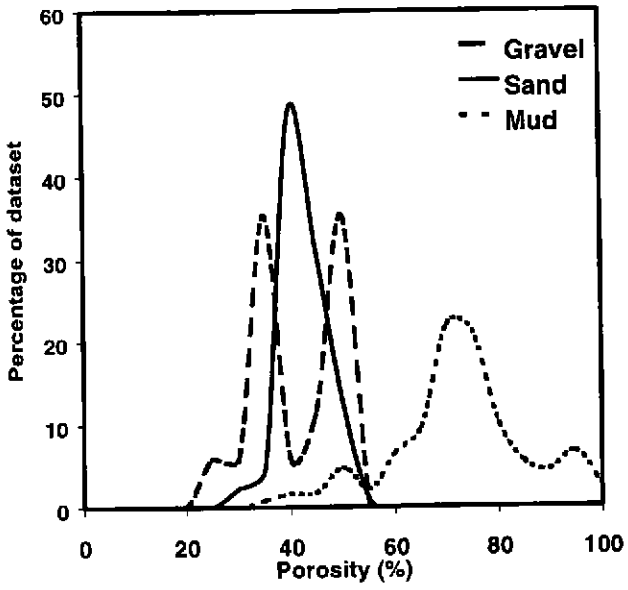

Figure 2. Porosity histograms for sediment types.

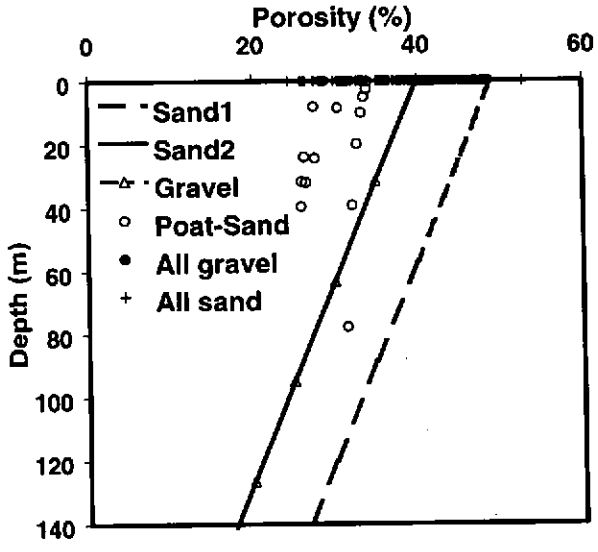

Figure 3. Porosity-depth relations for coarse sediments

2.3 Rock Model (Model Number 1)

The final model was for a typical rock outcrop at the seabed. Values from GEOSEIS were used to produce velocity, attenuation and density values for this model.

The nine models used are listed in Table 1, along with their acoustic properties at the sediment/water interface. The seabed types are listed in order of increasing porosity and, consequently, in order of decreasing sound speed. The lower number a seabed type is, the more reflective it is. The table gives four values of sound speed, one for each frequency of study. These values are deduced from a widely used expression [6] and show changes of about 2% over the range of frequencies used in the inversion studies. The "standard mud" referred to in the table is based on the values proposed by Baldwin and Butler [2] and all other muds are referred to in terms of how much their porosity (P) varies from this standard.

Type	Name	Porosity (%)	Density (kgm^{-3})	Atten'n ($dB\lambda^{-1}$)	Vp 150 Hz (ms^{-1})	Vp 400 Hz (ms^{-1})	Vp 800 Hz (ms^{-1})	Vp 1600 Hz (ms-1)
1	Rock	14	2360	1.36	3613	3613	3613	3613
2	Gravel	40	1990	0.738	1760.6	1775.1	1786	1796.9
3	Coarse Sand	40	1990	0.738	1696.5	1710.5	1721	1731.5
4	Fine Sand	49	1841.5	0.738	1597.6	1610.8	1620.6	1630.5
5	P-30 Mud	53	1775.5	0.682	1541.8	1553.4	1563.3	1571.6
6	P-20 Mud	63	1610.5	0.682	1412.4	1423	1432.1	1439.6
7	P-10 Mud	73	1445.5	0.682	1357.4	1367.6	1376.3	1383.5
8	Standard Mud	83	1280.5	0.682	1348.2	1358.3	1367	1374.2
9	P+10 Mud	93	1115.5	0.682	1293.4	1303.1	1311.4	1318.3

Table 1. Seabed types used in the inversion study with surficial acoustic properties; Vp *denotes sound speed.*

3. Acoustic Inversion Method

The subject of inverting acoustic data to determine the ocean environment has received considerable study in recent years [1] with methods being developed that are mainly designed around large-aperture vertical arrays. These detailed inversion methods use the full complex pressure as a function of frequency and depth in the ocean to determine the structure of the seabed. This is achieved by comparing measured pressure with predictions made

by acoustic propagation models. Propagation model runs are performed using a spread of assumed environmental descriptions, with the description of the seabed being restricted to a number of parameters such as surficial sound speed, sound speed gradient, etc. The closeness of agreement between modelled and measured data is quantified for each of the assumed environments, and those corresponding to the closest fits are used to generate a new set of assumed environmental parameters. Propagation models are then run using these new descriptions and, once more, those corresponding to the closest fits are used to produce a third "generation" of environmental descriptions. This process is repeated and, in favourable circumstances, the process will "home in" on the correct environmental description after a number of cycles. Such full inversion approaches require specialist acoustic arrays. In addition, considerable amounts of computer power is needed to perform the propagation model runs and to implement mathematical methods to produce the next set of environmental descriptions based on the results of the previous generation. For these reasons, in terms of use at-sea by non-specialist vessels, their practical applicability is very limited.

The approach developed in the work described in this paper is different from more detailed methods, in that the seabed description has been reduced to a single variable, the number giving the seabed type from one to nine. With such a limited description, only nine propagation loss model runs are required, and the "inversion method" is simply a case of quantifying the agreement between measured and modelled data and determining which of the nine seabed types gives the closest agreement.

In non-research applications, it is unlikely that full complex acoustic pressure will ever be extractable from sonars. Instead, it is more realistic to expect acoustic intensity amplitude (and hence propagation loss) to be extractable. For this reason, the inversion method developed here compares measured and modelled acoustic intensity amplitudes. The spatially-averaged mean difference between intensities is used to quantify the disagreement between the results of measurement and modelling. The mathematical definition of the parameter, ε, is:

$$\varepsilon = 10\log_{10}[1+\delta/1-\delta] \qquad \delta = \frac{1}{N}\sum_{n=1}^{N}\left((I_{n1}-I_{n2})/(I_{n1}+I_{n2})\right) \tag{5}$$

where N is the total number of points at which comparisons are made, I_{n1} is the nth value of intensity in the measured data set and I_{n2} is the corresponding value of intensity in the modelled data. This measure gives small values for situations where the predicted intensity is a good, average fit to the measured data. However it lacks the fine detail observed in the measurements. It should be made clear that ε is not the average dB difference between measured and modelled propagation loss. However, if the two curves are identical in shape with an offset of Z dB then the value of ε calculated for them will be equal to Z numerically.

The idea behind the pragmatic inversion approach is to produce a seabed type that gives a good, average fit to measured acoustic data. It is therefore not necessary to produced detailed acoustic interference patterns in the modelled data. While such patterns are likely to be present in the measured data, the lack of precision in the seabed description means that their locations are unlikely to be predicted adequately in the modelled data. One model allows the user to request the production only of range-smoothed data. This model is SUPERSNAP [9] and this ability led to the model being selected for use in this study. The model has a further advantage: its mathematical basis is not subject to any restrictions on the water depths and frequencies for which it is valid, as is the case for some other propagation models.

The environmental data required for a propagation model run, other than the seabed type, are assumed to be known precisely and are input directly to the propagation model. These data include water depth, wind speed and seawater sound speed.

Propagation loss model runs are performed for all nine seabed types, in combination with the other environmental parameters. The results from these runs are then used to produce nine values of ε. The seabed type that results in the smallest absolute value of ε is taken to be the best description of the seabed. Other information is gained by noting the seabed types that give the smallest value of ε but of opposite sign. Thus, if the closest fit is a negative value of ε, then the smallest positive value of ε is also noted. In this way, the two seabed types that bound the ideal, zero-error value are identified.

The seabed inversion method is tested here using a set of experimental data gathered in the Shelf Edge Studies Acoustic Measurement Experiment, SESAME, carried out in the late summers of 1995 and 1996 in the Northwest approaches to the UK, close to the Hebrides Terrace Seamount [10]. The experiment included acoustic measurements made in a well-characterised ocean environment. Environmental characterisation included seabed cores gathered during the acoustic propagation trials. Only a very small subset of the data was used in this study. This subset gave propagation loss versus range data gathered from a vertical line array spread over most of the water column. The array was made up of 31 hydrophones and propagation loss was determined for sources of frequencies of 150 Hz, 400 Hz, 800 Hz and 1600 Hz. Acoustic sources were deployed from a slowly drifting ship

whose range from the measurement array varied between 3 km and 20 km. The sound speed profile observed in the area is typical of late summer conditions with a surface mixed layer overlying a thermocline. Below this thermocline, an isothermal layer extended to the seabed. The acoustic sources used in the experiment were deployed at a depth of 50 m, close to the bottom of the thermocline. This configuration resulted in the dominant paths of sound from source to receiver being repeatedly reflected off the seabed. Previous studies [11] have shown that the ocean environment covered by this data can be represented as being effectively range independent, while still obtaining predictions that agree with the measured data to rms. errors of the order of 3dB.

The SESAME dataset is of high quality in both its acoustic and environmental data, and is ideal as a test case for the pragmatic seabed inversion method. The seabed type predicted by the inversion method is compared with the seabed data gathered during the experiment, allowing the accuracy of the inversion to be assessed. This comparison is only useful because of the high quality of environmental information available for the SESAME area. Without such ground truth data, an absolute assessment of the accuracy of the pragmatic inversion method would not be possible.

Seabed inversions are initially carried out using data measured by even-numbered hydrophones. Seabed type is calculated separately for the four source frequencies and the results compared to assess the frequency stability of the inversion method. Next, the process is repeated for data measured on the odd-numbered receivers in the array. This was done to investigate the stability of the inversion method to a change that should have no effect on its result. The *raison d'etre* of the pragmatic inversion method is to avoid the need to use large vertical line arrays. Consequently the next test of the method is to use only the top two receivers in the array in order to investigate whether the inversion method can correctly deduce the seabed type without the need for a large vertical array.

All the tests described above use data from the entire 17 km range of the measured acoustic data. The last test compares inversions made using the two shallowest receivers over the whole range extent with inversions made using data from only the first 20% (4 km) and the last 20% of the range extent of the data. This is done to investigate the possibility of deducing the seabed type using data gathered over small range windows.

4. Results

4.1 Inversions Using Whole VLA, Even-Numbered Receivers

The results of these calculations are shown in Table 2. The smallest value of the error function for each frequency, i.e. the value associated with the best match seabed, is highlighted in the table. The thick lines between cells show the transition from positive to negative values of the error function. The results in the table show that, for 150 Hz, the inversion method gives the seabed as being type 2, i.e. gravel. The error for this seabed type is equivalent to a mean error of less than 1 dB, indicating good agreement between the measured and modelled intensities. The closeness of the agreement is further indicated in Figure 4, which shows contours of measured and modelled propagation loss for the 150 Hz case.

	WHOLE VLA. EVEN-NUMBERED RECEIVERS								
	Seabed Type								
Freq. /Hz	T1	T2	T3	T4	T5	T6	T7	T8	T9
150	3.8	**-0.7**	-1.6	-3.9	-4.6	-14.8	-15.5	-15.8	-18.0
400	4.3	**-0.1**	-0.9	-3.1	-5.2	-45.6	-22.7	-35.4	-34.3
800	5.8	1.7	**1.0**	-1.1	2.9	-34.0	-40.0	-38.7	-33.2
1600	9.8	6.4	5.7	3.8	**1.9**	-53.0	-49.0	-47.0	-42.0

Table 2. Values of ε for each seabed type using whole extent of vertical line array. Smallest errors are highlighted for each frequency. Thick lines indicate the boundary over which the error changes from positive to negative.

While the fine detail of the measured data is not reproduced in the model results, the spread of data are similar, as shown by the highest and lowest contours used in the two plots. Figure 4 also shows contours of the difference between the measured and modelled data, and indicates that there is no trend in the spatial distribution of errors. Also shown in the figure are curves of measured and modelled loss versus range for the middle receiver used in the inversion. These curves show that the modelled data is producing a good, smoothed fit to the measurements. Further insight into the quality of the measured-modelled match can be obtained by treating as random the difference data shown in the lower left of Figure 4. If this data is used to produce a probability distribution function (pdf), the spread of errors can be determined. Figure 5 shows such a plot and indicates that the most frequently occurring errors are those close to a value of zero dB and that the half width of the distribution is of the order of 3 dB. Figure 5 also shows that the shape of the pdf is, approximately, Gaussian. Table 2 shows that, for the 400 Hz source, the inversion method gave the same results in terms of the seabed type resulting in the lowest error (gravel) and the location of the transition from positive errors to negative errors (between gravel and rock).

The seabed data gathered during SESAME showed that the seabed type in the area covered by the acoustic data was indeed gravel [10]. Thus, the inversion carried out at 150 Hz and 400 Hz was shown to determine the same seabed type as measured at sea by coring.

Table 2 shows that, for frequencies 800 Hz and 1600 Hz, the result of the inversion method is different from the low frequency cases. As frequency increases, the inversion drifts to the right in the table, towards the higher porosity sediments. At the frequencies dealt with here, these seabeds represent higher bottom losses. Not only does the inverted seabed type change, but the size of the errors also increases for the higher frequencies.

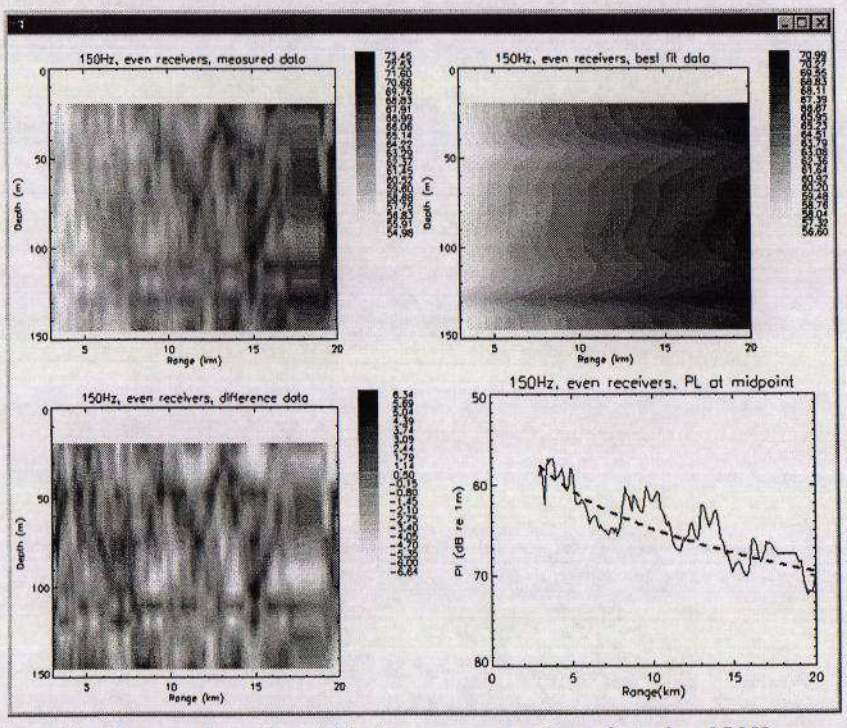

Figure 4. Measured and modelled propagation loss data for 150Hz source, even numbered receivers

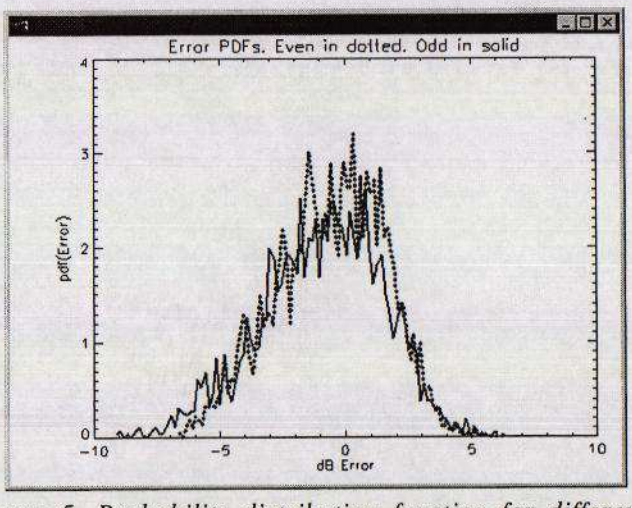

Figure 5. Probability distribution function for difference between measured and modelled propagation losses for 150Hz receiver.

Figure 6 shows contours of measured and modelled propagation losses at 1600 Hz and contours of the difference between the two. It can be seen that the difference data in this case has a definite distribution with position. This behaviour is different from the lower frequency cases, and indicates that the match between measured and modelled propagation loss is poorer at the higher frequencies. This is shown in the loss versus range curves in Figure 6, where it can be seen that the modelled curve is consistently above the measured data at short range. The poorer fit between measured and modelled data at higher frequency is further illustrated by the pdf of the difference between measured and modelled data, shown in Figure 7. The differences are distributed in a non-Gaussian pdf with a larger spread than was the case for the lower frequencies

There are two possible causes for the divergence of the inversion method at the two higher frequencies. The first is the possible presence of a thin mud layer on top of a gravel seabed. Such a structure is entirely possible in practice, but cannot be included in the standard seabed models without making them too complex for practical use. If such a layer was present, and was of the order of a few metres thick, it would be acoustically transparent to the lower frequencies whose wavelengths (10 m and 3.75 m respectively) would be too large to resolve it. It would, however, begin to become acoustically significant at the higher frequencies where its thickness would correspond to a larger number of wavelengths. Thus, if such a layer were present, it might result in the behaviour observed, whereby the inversion method gives more muddy seabeds at higher frequencies.A second explanation is associated with sea surface reflection losses. These are negligible at low frequencies but can be important at the two higher frequencies studied. The propagation model SUPERSNAP allows the inclusion of surface losses but assumes that the losses are inherently small. This is valid for low frequencies or very low wind speeds, but is wrong when the average sea surface height is of the order of, or greater than, an acoustic wavelength.

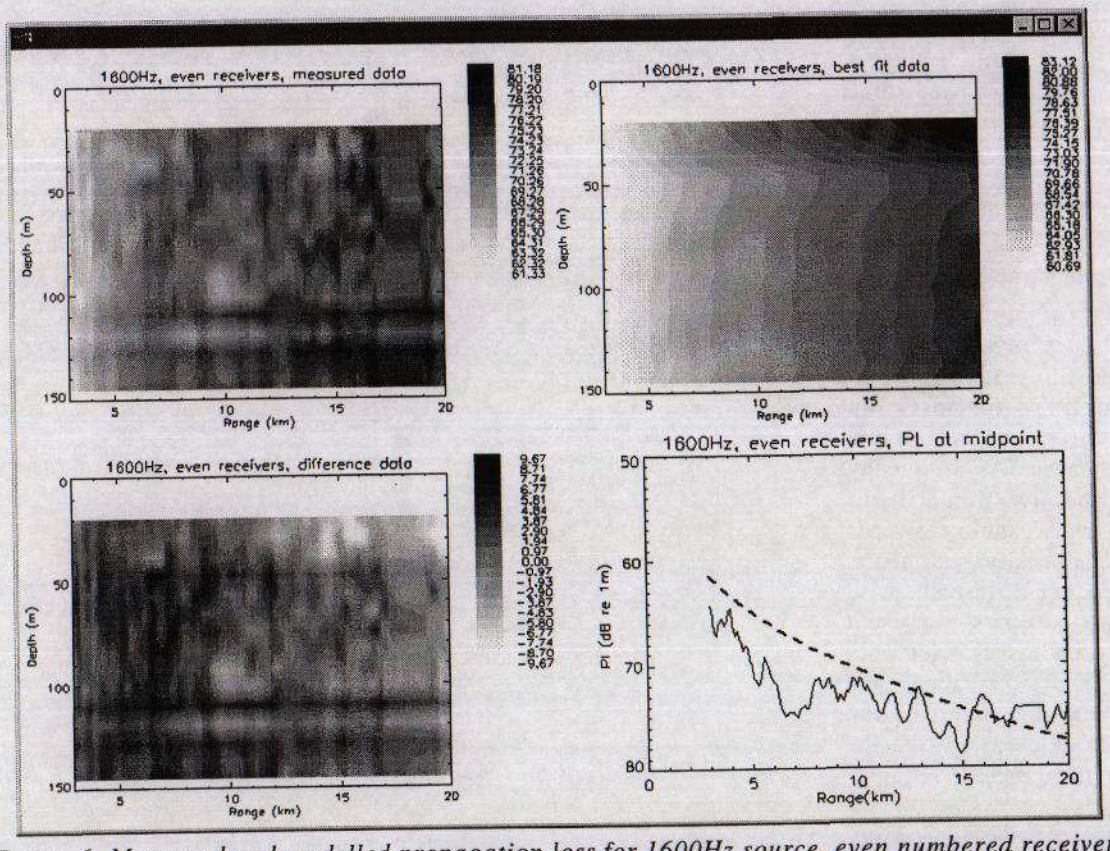

Figure 6. Measured and modelled propagation loss for 1600Hz source, even numbered receivers

The experimental situation had a windspeed of 17.5 knots and this is high enough for SUPERSNAP to underestimate surface losses. In such circumstances, if the correct seabed type were to be used, the modelled propagation losses would be lower than the measured ones. Closer agreement might be observed between the measurements and modelled data calculated using a less reflective seabed than was realistic. Thus, an unrealistically low value of surface loss results in the inversion method settling on a seabed type with too low a reflectivity

Inversions carried out for odd numbered receivers show the same results as the even numbered results, in terms of the seabed inverted for and the location of the transition from positive to negative errors. This illustrates the robustness of the inversion method to a change that should, and did, have no effect.

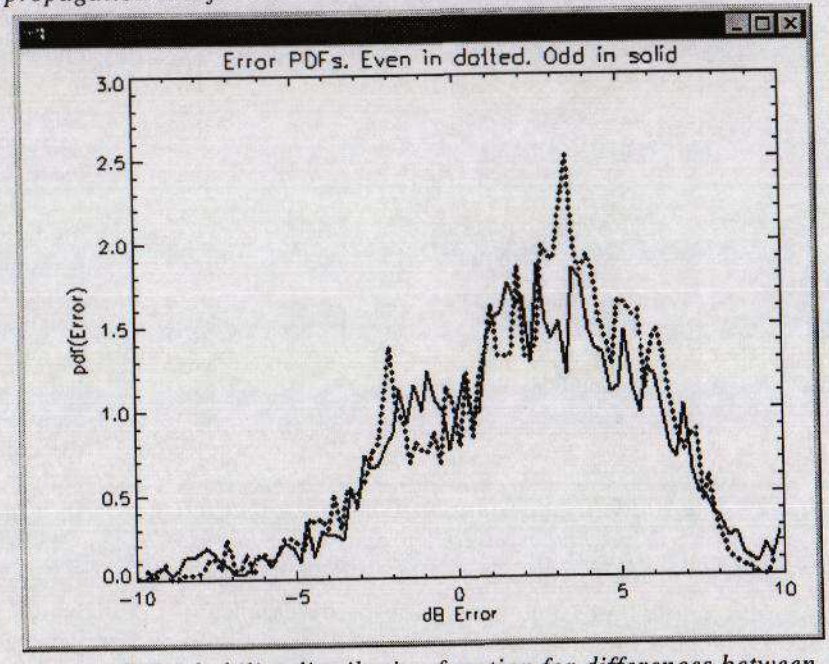

Figure 7. Probability distribution function for differences between measured and modelled propagation loss for 1600 Hz source, even numbered receivers.

4.2 Inversions Using Shallow Receivers Only

The idea behind using a pragmatic approach to inversion was that it might be possible to use it to design a seabed inversion system that could work using non-research sonars. The results shown in previous sections, while demonstrating the concept of pragmatic inversion, still utilize large aperture vertical arrays that are unlikely to be deployed outside specialist research applications. For this reason, the use of a smaller number of receivers was investigated. The two shallowest receivers were chosen because any operational system is more likely to be able to deploy shallow receivers than it is to use deeper systems. The results of the inversions are shown in Table 3.

		TWO SHALLOWEST RECEIVERS								
		Seabed Type								
Frequency/Hz		T1	T2	T3	T4	T5	T6	T7	T8	T9
150	Odd	**2.0**	-2.7	-3.7	-6.5	-7.0	-22.9	-24.3	-28.0	-24.4
	Even	3.4	**-1.5**	-2.6	-5.8	-6.9	-24.5	-26.2	-30.4	-26.1
400	Odd	3.0	**-1.5**	-2.5	-5.3	-8.4	-45.8	-45.6	-47.0	-43.9
	Even	3.7	**-1.0**	-2.1	-5.1	-8.6	-45.6	-52.8	-50.0	-49.5
800	Odd	4.2	**-0.1**	-1.0	-3.5	-6.0	-67.4	-65.2	-63.4	-67.4
	Even	5.6	1.0	**0.0**	-2.7	-5.3	-65.7	-75.2	-70.4	-70.4
1600	Odd	8.2	4.4	3.5	1.3	**-1.1**	-Inf	-Inf	-Inf	-Inf
	Even	9.2	5.3	4.4	1.9	**-0.7**	-Inf	-Inf	-Inf	-Inf

Table 3. Values of ε for each seabed type using only the two shallowest receivers. The smallest errors are highlighted for each configuration. Thick lines indicate the boundary over which the error changes from positive to negative

The inversions using the shallowest receivers are similar to the results using the whole array. For frequencies of 150 Hz and 400 Hz, the seabed type produced by the inversion is type 2 (gravel) in all but one case. For the two higher frequencies, the "drift to the right" in the inversion results is the same as for the whole array results. Thus, if only the shallowest two receivers in the array are used in the inversion, the seabed type predicted is not significantly changed from the inversions made using the full water column array.

4.3 Inversions Using Shallow Receivers With Limited Range Extents

It would be advantageous if the seabed type could be deduced from acoustic measurements made over distances of the order of a few kilometres, rather than the 17km used in the previous inversions. To investigate the feasibility of this, inversions are performed using the two shallowest receivers in the array over range windows covering initially only the first 20% and then the last 20% of the total available.

		TWO SHALLOWEST RECEIVERS, LIMITED RANGE WINDOWS								
		Seabed Type								
Frequency/Hz		T1	T2	T3	T4	T5	T6	T7	T8	T9
150 Short	Odd	2.4*	**-1.5**	-2.2	-4.2	-4.8	-17.0	-18.4	-22.7	-18.1
	Even	3.7	**-0.33***	-1.2	-3.3	-4.3	-18.5	-20.2	-25.0	-19.8
150 Long	Odd	**1.7***	-3.9	-5.2	-9.2	-9.3	-35.8	-37.0	-36.7	-43.9
	Even	3.5	**-2.3***	-3.7	-8.2	-9.5	-38.4	-39.7	-39.5	-46.5
400 Short	Odd	**1.8**	-1.9*	-2.6	-4.6	-6.7	-38.8	-39.3	-40.0	-37.0
	Even	2.5	**-1.5***	-2.2	-4.4	-6.8	-38.6	-46.2	-43.0	-42.6
400 Long	Odd	4.8	**-0.5***	-1.7	-5.3	-9.7	-Inf	-60.7	-Inf	-Inf
	Even	3.5	**-2.3***	-3.7	-8.2	-9.5	-38.4	-39.7	-39.5	-46.5
800 Short	Odd	3.6	**0.0***	-0.6	-2.5	-4.4	-60.7	-57.8	-56.2	-60.4
	Even	5.0	1.3	**0.6***	-1.4	-3.3	-59.1	-66.2	-62.4	-64.8
800 Long	Odd	4.7	**-0.3***	-1.5	-4.7	-8.2	-Inf	-Inf	-Inf	-Inf
	Even	6.8	1.4	**0.1***	-3.4	-7.0	-Inf	-Inf	-Inf	-Inf
1600 Short	Odd	9.0	6.0	5.4	3.6	**1.7***	-Inf	-Inf	-Inf	-Inf
	Even	10.4	7.5	6.8	5.1	**3.0***	-Inf	-Inf	-Inf	-Inf
1600 Long	Odd	7.2	2.7	1.7	**-1.0**	-4.5*	-Inf	-Inf	-Inf	-Inf
	Even	8.3	3.7	2.6	**-0.5**	-4.5*	-Inf	-Inf	-Inf	-Inf

Table 4. Values of ε for each seabed type using only the two shallowest receivers. The smallest errors are highlighted for each configuration. Thick lines indicate the boundary over which the error changes from positive to negative. Asterisks mark the seabed types inverted for using the whole range of data.

Table 4 shows the error values for each seabed type, as a function of frequency, for even and odd receivers at long and short ranges. The asterisks show the seabed type previously inverted for using the whole range of the data. The results for the inversions at the lowest two frequencies show little variation between odd and even results. The transition from positive to negative errors occurs in the same place (between types 1 and 2) for all inversions at 150 Hz and 400 Hz and in only one case (150 Hz, long range, odd numbered receivers) does the inversion diverge markedly from seabed type 2. The table shows that in all but two cases, the seabed inverted for using the subset of the range data was the same as that inverted for using the whole range extent of the data. At the two higher frequencies, the inversion is more erratic and less robust to changes between odd and even receivers. The "drift to the right" in the results observed for the full range inversion is again present for the short- and long-range inversions.

5. Conclusions

Geophysical information has been used to define nine seabed types which, while not containing all possible geological detail, are proposed to be a good description of the bulk details of the seabed in the majority of ocean conditions. A method has been developed that allows the seabed to be classified as one of these nine types on the basis of acoustic measurements made in the ocean. Unlike other, more precise, methods this pragmatic inversion method does not rely on complicated research sonars to measure the full complex pressure. Instead, any apparatus capable of determining propagation loss could be used as a source of acoustic data for the pragmatic inversion to yield a seabed classification.

6. Acknowledgements

The authors thank all the SESAME trials team whose hard work made possible the analysis reported here.

References

[1] Jensen FB, Kuperman WB, Porter MB and Schmidt H. Computational Ocean Acoustics AIP Series

[2] Baldwin B and Butler, C.O. Compaction Curves. *Am Assoc. Pet Geol Bul.* 1985; **69**: 622-625

[3] Graham CC. User guide for PROGEN and SEISTOOL, V1.0. BGS Technical Report WB/95/26C 1995

[4] Marks SG. Variation of sediment properties with depth and application to GEOSEIS algorithms Unpublished DERA Report

[5] McCann C, Assefa, SB, Sothcott J and McCann DM, Seismic properties of sea floor sediments and rocks: GEOSEIS version 2. University of Reading P.R.I.S. publication no 509/BGS Report No. 96/13/C. 1996.

[6] Marks SG. A seabed handbook. DERA/SSPS/CR97022/1.0. May 1997

[7] Sclater JG and Christie PAF. Continental stretching: an explanation of the post-mid-Cretaceous subsidence of the central North Sea Basin *J. Geophys. Res* 1980; **85:** 3711-3739

[8] Poat CM. Geotechnical and geophysical properties of typical beach overburden materials, Anglesey. A comparison of modelled and field data. MSc Thesis, University of Wales, Bangor 1991

[9] Jensen FB. Numerical Models In Underwater Acoustics In *Hybrid Formulations Of Wave Propagation And Scattering* Felsen LB (3d.), NATO ASI Series. Martinus Nijhoff Publishers. Pp. 295-335

[10] Kelly KM, Marks SG, Prior MK, Scott JC and Small J. SESAME Data Analysis Report. DERA/SSPS/CR980031/1.0. 1998.

[11] Prior MK, Marks SG, Devonshire E, Sawyer T. Comparison Of Measured And Modelled Underwater Acoustic Propagation Loss On The Malin Shelf. In *Underwater Defence Technology (UDT) 2000.* P11.8.

Geoacoustic inversion using long range reverberation

D. A. Miles, S. D. Richards, G. C. Searing, E. D. Stevens, K. R. Williams

Defence Evaluation & Research Agency, DERA Winfrith, Winfrith Technology Centre, Dorchester, Dorset, DT2 8XJ, UK. dmiles@dera.gov.uk

Abstract

Inversion of active sonar reverberation returns offers the potential for inferring geoacoustic properties of the seabed. Reverberation levels from seabed scattering are affected by the propagation to and scattering from the seabed, the important geoacoustic parameters being sediment sound speed, attenuation, and density. Bottom scattering has been modelled using Lambert's Rule; therefore Lambert's parameter is also part of the forward model parameterization. Global inversions for these parameters are performed on synthetic data using a genetic algorithm and a downhill simplex method. The results show that it is possible to infer geoacoustic properties for synthetic environments, with similar results being obtained from both of the methods used.

1. Introduction

Reverberation returns from active sonar transmissions contain information about the environment surrounding the source and receiver. In shallow water, propagation at all but very short ranges will include the effects of multiple surface and bottom interactions, and the nature of the interfaces will affect both surface and bottom reverberation. Long-range reverberation will therefore contain information about the environment over a considerable region and the aim of this work is to obtain information about the seabed from such reverberation returns. Initial work reported here is concentrated on inverting synthetic data for range-independent environments, but the intention is to extend this approach to include the effects of range-dependent environments.

2. Methodology

2.1 Introduction

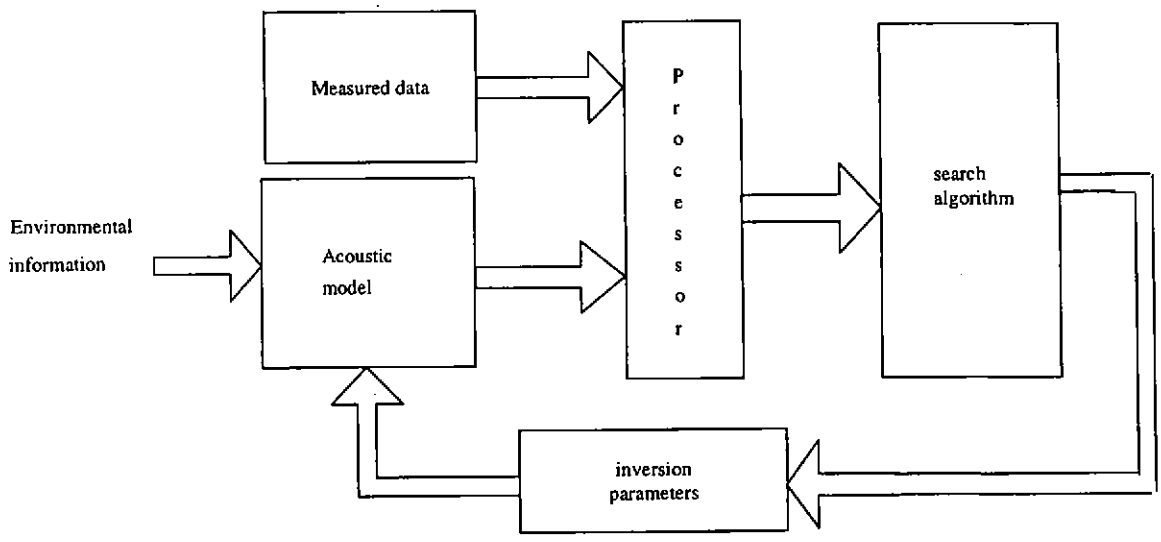

Figure 1. Block diagram of inversion process

In this section the methodology adopted for inversion studies is described. Results to date are concentrated on full inversion of seabed parameters at 1 kHz in a synthetic shallow water, range-independent environment. Both a local search method (downhill simplex) and a global method (genetic algorithm, GA) are utilised. The software package SAGA [1] is used to perform the GA based searches. The downhill simplex method is implemented using code developed by the authors. Figure 1 illustrates the basic inversion process and each component illustrated is described below.

2.2 Environment Information, Acoustic Model and Measured Data

Three synthetic environments were selected to represent typical seabed sediment types. All environments are shallow water, with a water depth of 100 m, and with range independent properties. The seabed is defined as a homogenous half-space with a density ρ, attenuation α and compressional sound speed v, as given in Table 1. Seabed scattering is modelled by Lambert's Law [2], with the level determined by the Lambert constant μ. Sea surface reflection loss is modelled using a modified form of the Marsh-Shulkin-Kneale relationship [3,4], and sea surface scattering is modelled using the Chapman-Harris formula [5]. A wind speed of 5 ms^{-1} is used. A downward refracting sound speed profile was chosen to ensure that reverberation from the sea surface is small compared to that from the seabed. In all cases the source and receiver are omnidirectional with the source at a depth of 50 m and the receiver at a depth of 20 m. The frequency used is 1 kHz.

Environment	v (ms^{-1})	α ($dBm^{-1}kHz^{-1}$)	ρ (kgm^{-3})	μ (dB)
Sand	1710.8	0.31	1994	-27.0
Sandy gravel	1790.3	0.80	1998	-27.0
Muddy sand	1627.7	0.30	1800	-27.0

Table 1. Synthetic environments

Work has previously been reported using SAGA to invert reverberation data [6] using a normal mode model [7] that is incorporated into SAGA. For this work we have chosen to use the Instant [4] model owing to its ability to be extended to model range-dependent environments. The model is used to generate the synthetic ('measured') data as well as being used as the forward model during the inversion process.

2.3 Processor

All studies carried out in this paper use the cost function,

$$\phi = \sum_{i=1}^{N} \left(\frac{|p_i|}{\sqrt{\sum |q_i|^2}} - \frac{|q_i|}{\sqrt{\sum |q_i|^2}} \right)^2 , \qquad (1)$$

where p and q are the measured and modelled total reverberation (in dB re 1μPa) respectively summed over the N points of the data. The value of this function indicates the degree of matching between the measured and modelled data, where a value of zero indicates a perfect match. It is common to refer to the value of the cost function as the energy.

2.4 Search Algorithm

Inversion can be thought of as an optimization of an n dimensional function, where n is the number of parameters to be determined and the function is a comparison of the modelled to measured data. If n is small then an exhaustive search of the space can be carried out to determine the global minimum, which corresponds to the true solution. However, as the number of parameters increases, the size of the search space increases exponentially and exhaustive methods rapidly become prohibitively slow. Therefore other search methods have to be sought. There are local methods available that progress until a minimum value for the function is found. However, in most high dimensional problems the function space has multiple local minima (multi-modal) preventing local search techniques from finding the global minimum. To overcome this problem many inversion schemes employ global search strategies, such as simulated annealing or genetic algorithms that are capable of escaping from these local minima. The performances of both a global search method (GA) and a local search method (downhill simplex) are investigated and the results compared.

2.5 Inversion Parameters

Since the intention of this work is to obtain information about the seabed from reverberation returns, inversion is undertaken to obtain only those parameters that describe the seabed. It is therefore assumed that information

about the wind speed, sonar deployment depths, sound speed profile and water depth, are known. The resulting inversion parameters are seabed sound speed v, density ρ and attenuation α, which affect bottom reflection loss and hence propagation, and the Lambert's parameter μ, which controls the level of bottom scattering.

3. Inversion Parameter Ambiguities

3.1 Two-dimensional Ambiguities

Before attempting to invert synthetic data, it is instructive to analyse both the sensitivity of reverberation to the various parameters and the correlations between parameters. This is achieved by calculating the ambiguity surfaces for pairs of the parameters μ, α, ρ, and v. Figure 2 shows ambiguity plots between pairs of parameters for the sand environment; results for the other two environments are qualitatively similar. As can be observed, the energy is low around the true solutions (white regions) while away from the true solution the energy is high (dark regions).

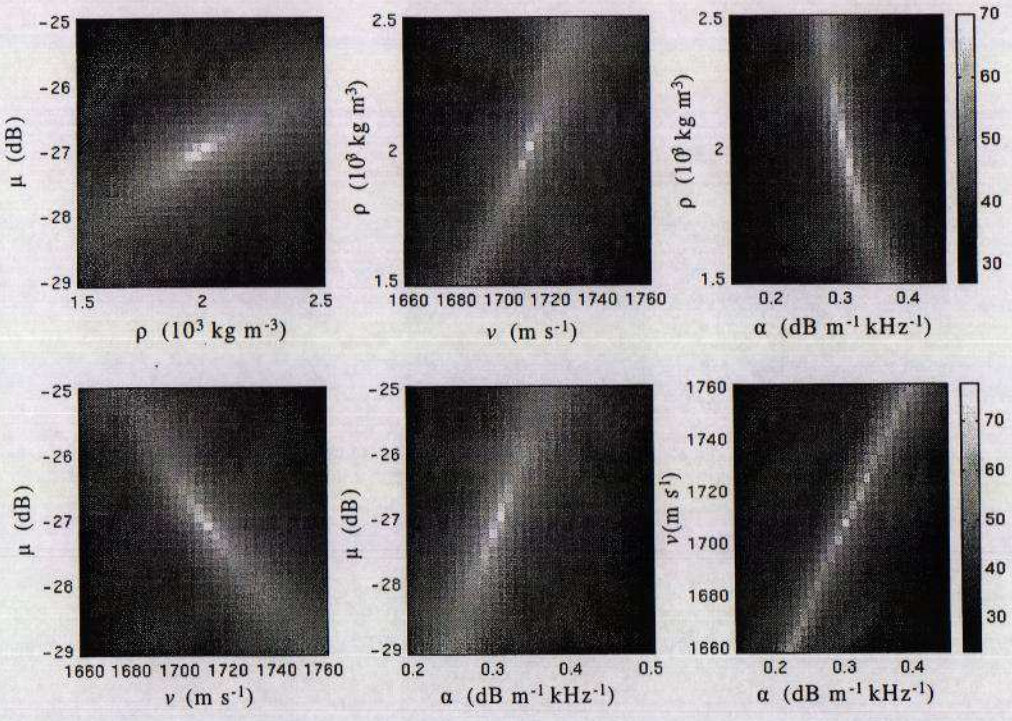

*Figure 2. 2D parameter ambiguities for sand environment. The grey scale shows -10*log$_{10}$(energy).*

The correlations observed in Figure 2 present two major problems to an inversion scheme. First, GAs have problems navigating spaces with strong correlations. Collins and Fishman [8] suggest that a new set of parameters can be formed to align with the line of minimum energy so that the GA can locate the true minimum. Second, when noise is present in the data the true solution can become lost and a unique solution may no longer be found. This defines a fundamental limit on the resolution of the parameters for any inversion scheme. How easily the solution becomes lost depends on how sharp the line of minimum energy is, and how sensitive the cost function is to noise. If the noise swamps the minimum completely there is little point aligning a new set of parameters to the line of minimum energy since no unique minimum exists.

The strongest correlation exists between the half-space sound speed and attenuation. This is true for each of the environments. However, closer inspection reveals that the gradient of the line of minimum energy is different for each case and therefore related to the seabed type. Another feature of the ambiguity plots is the presence of multiple minima. These can cause problems for the downhill simplex method, since it is a local based search algorithm and can become stuck on any one of them. These pictures only give a simple 2D picture of parameter correlations; since the true relationships exist in a 4D space, correlations between three or more parameters may not be evident.

3.2 Sediment Sound Speed-Attenuation Ambiguity

In shallow water at medium and at long ranges the only important propagation paths are those at shallow angles, often only those well below the critical angle. In this region bottom reflection loss increases linearly with grazing angle. In these

cases, bottom reverberation level is therefore only sensitive to the value of this slope, and not directly related to the value of the critical angle. The value of this slope is given by,

$$\eta = \frac{\rho\alpha(\cos\theta_c)^2}{\pi(\sin\theta_c)^3}, \tag{2}$$

where θ_c is the critical angle [9]. Figure 3 shows the ambiguity between half-space attenuation and sound speed for the synthetic sand environment. The line $\eta = const$ (where the constant value is calculated from the true values of the sediment parameters ensuring that the line goes through the true solution) is superimposed and coincides with the ambiguity. The location of the minimum along the ambiguity, denoted by ξ, is not easily resolvable whereas the location and orientation of the ambiguity, denoted by the η, is resolvable. As can be observed in Figure 3 there is a well-defined white spot which uniquely resolves both the half-space attenuation and sound speed. However, the figure shows synthetic data to which noise has not been added and the addition of noise may cause the location of this minimum along the ambiguity to become lost.

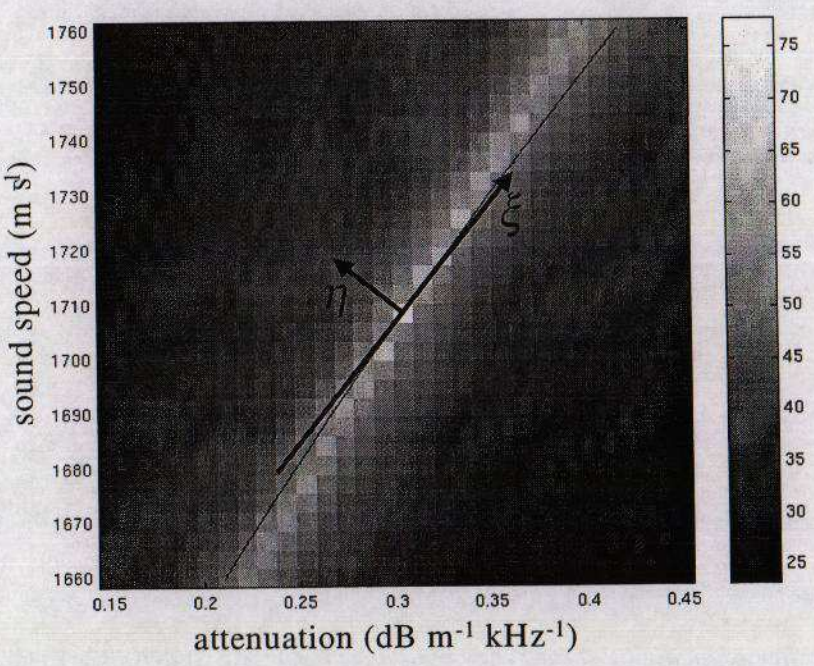

Figure 3. Sediment sound speed-attenuation ambiguity for sand environment.

4. Results

4.1 Inversion Using Genetic Algorithm

The software package SAGA is used to invert for the seabed attenuation, sound speed, density and Lambert's parameter. This is repeated five times for each synthetic environment, each time using a different randomly selected initial population of trial solutions. After the inversions are complete for each synthetic environment, the parameter combination corresponding to the best fit (lowest energy) is taken as the solution to the problem. Examination of the results shows that the parameter combination yielding the lowest energy generally corresponds to the best solution. Means and standard deviations of the best-fit parameters have been calculated to give a rough estimate of the success of the inversions. These are shown in Tables 2 to 4. In addition to the four inverted parameters v, α, ρ, μ the value of η is also given.

It is encouraging to see that, even with the wide spread of values for v and α, the estimate of η is good for all three environments. As explained in section 3.2, the reverberation is most sensitive to the bottom loss gradient η and not the individual values of v, α and ρ.

SAND	True	Mean	Standard deviation	Best of all
ρ (10^3 kg m^{-3})	1.994	1.860	0.15	1.9
μ (dB)	-27.0	-27.18	0.48	-27
v (m s^{-1})	1710.8	1799.4	57.42	1708
α (dBm^{-1}kHz^{-1})	0.31	0.49	0.10	0.31
η (dB rad^{-1})	1.28	1.14	0.08	1.26

Table 2. Overall GA inversion results for sand environment

SANDY GRAVEL	True	Mean	Standard deviation	Best of all
ρ (10^3 kg m^{-3})	1.998	2.14	0.15	2
μ (dB)	-27.0	-27.25	0.39	-27
v (m s^{-1})	1790.3	1777	45	1791
α (dBm^{-1}kHz^{-1})	0.8	0.72	0.17	0.8
η (dB rad^{-1})	2.09	2.15	0.10	2.09

Table 3. Overall GA inversion results for sandy gravel environment

MUDDY SAND	True	Mean	Standard deviation	Best of all
ρ (10^3 kg m^{-3})	1.8	1.7	0.19	1.5
μ (dB)	-27.0	-27.25	0.58	-26.6
v (m s^{-1})	1627.7	1716	55	1708
α (dBm^{-1}kHz^{-1})	0.3	0.59	0.18	0.63
η (dB rad^{-1})	2.26	1.99	0.12	1.99

Table 4. Overall GA inversion results for muddy sand environment

The best-fit solutions (circles) for each of the five inversions for each synthetic environment are illustrated in Figures 4 to 6 (note the solid lines represent the true solutions). Large spreads in the values of α and v can be observed for all three environments. In each case α and v are strongly correlated and consistent with the ambiguities mentioned in section 3.1. These results highlight the difficulty a GA has navigating such surfaces. Observing Figure 4 and Figure 5 a clear minimum in the energy function is present. In any one inversion the GA is unlikely to locate this minimum, since it becomes stuck elsewhere on the ambiguity and unable to proceed along the line of minimum energy. This suggests that a re-parameterization of the attenuation and compressional sound speed in terms of the bottom loss gradient (η) would improve the performance of the GA for synthetic noise free environments.

The solution with the lowest value of cost function from all five inversions has been selected for each environment. This is labelled "Best of all" in Tables 2 to 4. The "best of all" value gives very good estimates of the geoacoustic parameters for the sand and sandy gravel environments. However, the muddy sand results are less encouraging. The lack of significant differences in energy between the five inversions illustrated in Figure 6 demonstrates why this method is unable to obtain more accurate values for the parameters.

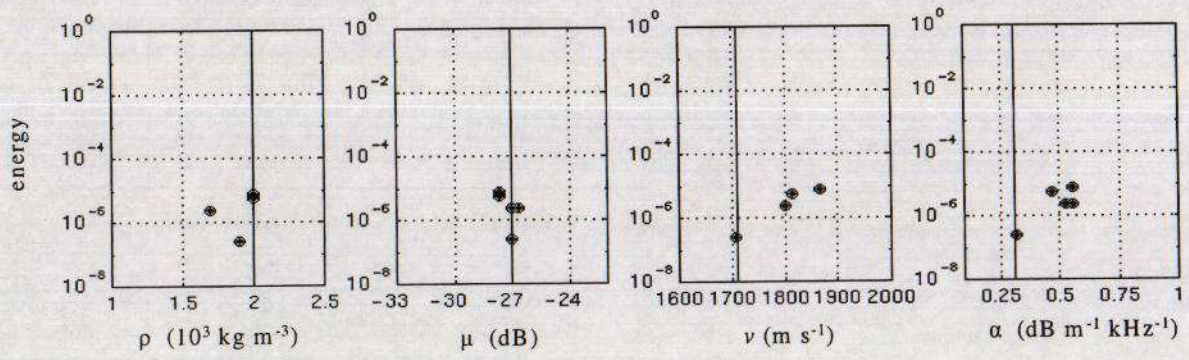

Figure 4. Best fits for each inversion for the sand environment. Individual data points represent the results of individual inversions. The solid vertical line represents the true solution.

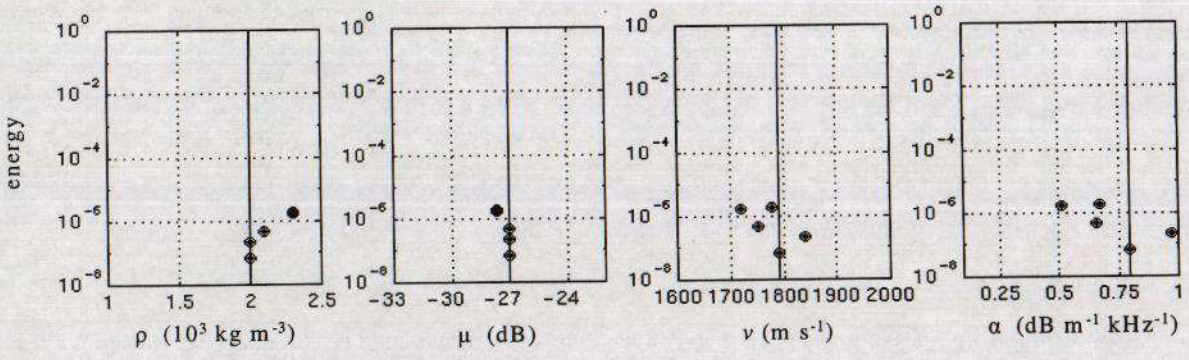

Figure 5. Best fits for each inversion for sandy gravel environment. Individual data points represent the results of individual inversions. The solid vertical line represents the true solution.

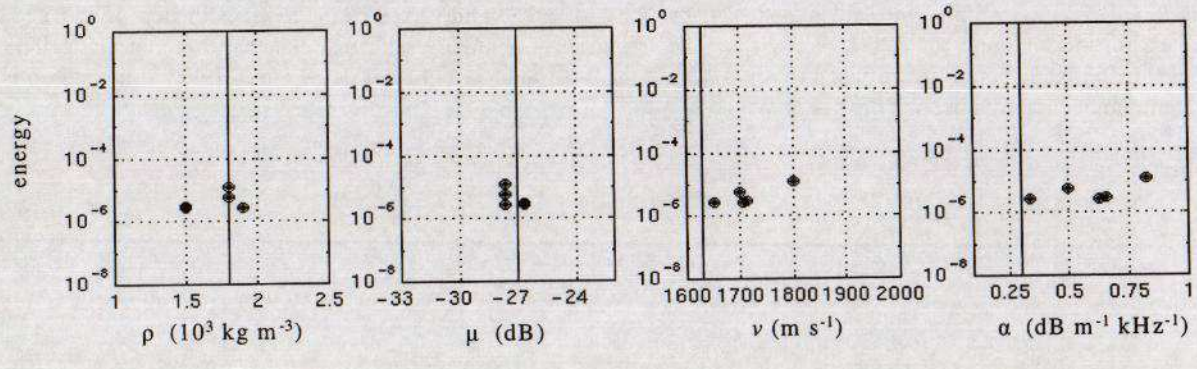

Figure 6: Best fits for each inversion for muddy sand environment. Individual data points represent the results of individual inversions. The solid vertical line represents the true solution.

4.2 Inversion Using Downhill Simplex Method

The studies undertaken for the GA are repeated using the downhill simplex scheme. As before, inversion of the four parameters is repeated five times using different random initial guesses for the simplex for each environment. The cost function being minimised is again defined by Equation 1.

SAND	True	Mean	Standard deviation	Best of all
ρ (10^3 kg m^{-3})	1.994	2.04	0.13	1.98
μ (dB)	-27.0	-27.1	0.09	-27
v (m s^{-1})	1710.8	1718	146	1704
α (dBm^{-1}kHz^{-1})	0.31	0.32	0.24	0.30
η (dB rad^{-1})	1.28	1.31	0.15	1.28

Table 5. Downhill simplex results - sand environment

SANDY GRAVEL	True	Mean	Standard deviation	Best of all
ρ (10^3 kg m^{-3})	1.998	1.93	0.19	1.99
μ (dB)	-27.0	-26.97	0.09	-27
v (m s^{-1})	1790.3	1781	58	1781
α (dBm^{-1}kHz^{-1})	0.8	0.79	0.17	0.77
η (dB rad^{-1})	2.09	2.09	0.08	2.11

Table 6. Downhill simplex results - sandy gravel environment

MUDDY SAND	True	Mean	Standard deviation	Best of all
ρ (10^3 kg m^{-3})	1.8	2.7	0.54	3.2
μ (dB)	-27.0	-29.3	0.30	-28.9
v (m s^{-1})	1627.7	1663	117	1669
α (dBm^{-1}kHz^{-1})	0.3	0.37	0.27	0.37
η (dB rad^{-1})	2.26	3.12	0.55	3.33

Table 7. Downhill simplex results - muddy sand environment

As in the case of the GA, the best of all parameters are selected for each of the environments and the results tabulated in Tables 5 to 7. For both the sand and sandy gravel environments the resolution of Lambert's parameter is much tighter than the GA results. However, the spread of the attenuation and compressional sound speed is larger. Broadly speaking the results for the sand and sandy gravel environments are similar to the GA. Again the attenuation and compressional sound speed are strongly correlated. It is likely that this spread is caused by the simplex method becoming stuck on local minima along the ambiguity surface. However, further investigation is needed. The results for the muddy sand environment are poorer than for the other environments and much worse than for the GA.

5. Conclusions

This study demonstrates that it is possible to determine, through inversion, the geoacoustic parameters used to generate synthetic reverberation time histories. Both GA based and local based search approaches were used. A marked spread in the results is evident for both methods, particularly for the attenuation and compressional sound speed. However, for the sand and sandy gravel environments, better resolution can be obtained if several inversions are performed and the lowest energy solution used. For both methods inversion is less successful for the muddy sand environment, although the results are better for the GA.

If the attenuation and compressional sound speed are re-parameterized in terms of the bottom loss gradient, an improvement in the performance of the GA for synthetic noise free environments would be expected.

Acknowledgements

The work contained in this paper was carried out as part of Technology Group 01 of the MoD Corporate Research Programme.The authors also wish to acknowledge valuable discussions with Dr. Mike Ainslie of CORDA.

References

[1] Gerstoft P. SAGA User Manual 2.0: An inversion software package, SACLANTCEN, SM-333, 1998

[2] Mackenzie KV. Bottom Reverberation for 530 and 1030 cps Sound in Deep Water , *Journal of the Acoustical Society of America*, 1961; **33**: 1498-1504

[3] Marsh HW, Schulkin M, and Kneale SG. Scattering of Underwater Sound by the Sea Surface, *Journal of the Acoustical Society of America*, 1961; **33**: 334-340

[4] Horsley GD, Ainslie MA, and Robins AJ. Bistatic Sonar Performance Model: User Guide, BAe, CR1156/TU-1, 2000

[5] Chapman RP and Harris JH. Surface Backscattering Strengths Measured with Explosive Sound Sources, *Journal of the Acoustical Society of America*, 1962; **34**: 1592-1597

[6] Ellis DD and Gerstoft P. Using inversion techniques to extract bottom scattering strengths and sound speeds from shallow–water reverberation data, in *Proceedings of the 3rd European Conference on Underwater Acoustics*, 1996

[7] Ellis DD. A shallow water normal mode reverberation model, *Journal of the Acoustical Society of America*, 1995; **97**: 2804-2814

[8] Collins MD and Fishman L. Efficient Navigation of Parameter Landscapes, *Journal of the Acoustical Society of America*, 1995; **98**: 1637-1644

[9] Weston DE, Intensity-range relations in oceanographic acoustics, *Journal of Sound and Vibration*, 1971;**18:** 271-287